Matrix cracking in polymeric composites laminates: Modelling and experiments

D.T.G. Katerelos [a,d,*], M. Kashtalyan [b], C. Soutis [c], C. Galiotis [d]

[a] *Polymer Engineering Division, Department of Applied Physics and Mechanical Engineering, Luleå University of Technology, SE 971 87 Luleå, Sweden*
[b] *Centre for Micro- and Nanomechanics, School of Engineering and Physical Sciences, University of Aberdeen, Aberdeen AB 243 UE, UK*
[c] *Department of Mechanical Engineering (Aerospace), The University of Sheffield, Sheffield S1 3JD, UK*
[d] *FORTH/ICE-HT, Stadiou str. Platani, Patras, P.O. Box 1414, GR-265 04, Greece*

Abstract

Composites ability to retain functionality in the presence of damage is a crucial safety and economic issue. Generally the first damage mode in composite laminates is matrix cracking, which affects the mechanical properties of the structure long before its load-bearing capacity is exhausted. In this paper, a detailed analysis of the effect of matrix cracking on the behaviour of cross-ply $[0/90]_s$ and unbalanced symmetric $[0/45]_s$ glass/epoxy laminates loaded statically in tension is performed. Theoretical predictions of stiffness reduction due to damage are based on the Equivalent Constraint Model (ECM), which takes into account concurrent matrix cracking in all plies of the laminate, although matrix cracking under consideration is developing only within the off-axis ply of the laminates. The longitudinal Young's modulus predictions are compared to experimentally derived data obtained using laser Raman spectroscopy (LRS). The good agreement between predicted and measured values of the reduced longitudinal Young's modulus validates the ECM model and proves that its basic assumptions are accurate. Thus, the predictions for all the mechanical properties by the ECM model are within a realistic range, while experimental evidence is required for further validation.
© 2007 Elsevier Ltd. All rights reserved.

Keywords: A. Polymer–matrix composites (PMCs); B. Matrix cracking; C. Damage mechanics; C. Transverse cracking; D. Raman spectroscopy

1. Introduction

Durability of a system is, in general, its ability to retain functionality during service life even though a certain amount of damage has developed. In structural elements manufactured with composites, durability is of primal significance and, thus, understanding of damage mechanisms is extremely important. The first mode of damage appearing is the accumulation of microdefects and failures within the weakest parts of a laminate (off-axis plies, interphases and interfaces). Matrix cracking, also known as intralaminar

cracking [1], or transverse cracking (in the case of layers oriented perpendicular to the loading axis), has been broadly investigated, both experimentally and theoretically. Experiments have shown that in the case of cross-ply standard test coupons the cracks are growing almost instantaneously spanning the total width of the specimen. General off-axis laminas behave differently in the sense that cracks are developed in a more stable manner with time and applied load. Cracking density depends on geometrical (layer orientation with respect to the load direction, laminate stacking sequence, ply thickness), material (mechanical properties and fracture toughness in particular) and loading (load level, temperature change, number of cycles in fatigue) parameters. Cracks are characterised by the opening and sliding of their surfaces, which reduce the average load-bearing ability of the damaged lamina and consequently reduce the laminate thermo-elastic properties.

Matrix cracking and its effect on material properties degradation has been investigated by many researchers, see, e.g., reviews [1–5]. In most cases the effort has been focussed on the development of a representative local stress distribution model between the cracks, which is then used to determine certain thermo-elastic constants. Shear-lag analyses and variational models are the most widely used approaches, with the Hashin's variational model [6] being simple and consistent, although rather inaccurate in the case of large cracked layer thickness. McCartney and Schoeppner [7,8] have proposed most exact solutions involving complex numerical routines. In most cases the models are restricted to the prediction of some elastic parameters (mainly the longitudinal laminate Young's Modulus, E_x) of a general cross-ply composite system. Numerical approaches, such as the finite elements method are used to derive theoretical predictions for comparison to experimental data regarding to both cross-ply and more complex laminate systems [9–11]. The crack face relative displacements as the governing parameters of the stiffness reduction are used in [12,13]. This approach is based on neglecting the neighbouring layers effect on crack face displacements and using known solutions for a periodic system of cracks in an infinite homogeneous transversely isotropic 90° layer, rendering in quantities independent on the relative ply stiffness ratios. A modified but simpler model based on crack face displacements (crack opening displacement, COD and crack sliding displacement, CSD) and accounting the cracks interaction is proposed by Varna and Lundmark [14,15]. The model contains material properties, geometrical characteristics and the aforementioned microscale parameters, COD and CSD normalised to the applied stress. In order to analyse multidirectional laminates with multiple damaged layers and to take into account the effect of in-situ constraint on the damage in a particular lamina, an approach based on the Equivalent Constraint Model (ECM) of the damaged laminate was proposed in [16,17]. Instead of the original damaged laminate, it was suggested to analyse simultaneously a set of ECM laminates, in each of which all the laminae below and above a particular damaged lamina have been replaced with homogeneous orthotropic layers having the equivalent constraining effect. This approach was verified in [16,18] by comparison with other theoretical models and successfully applied to analysis of cross-ply [16] and angle ply [17] laminates.

In the present paper an attempt to understand the effects of damage on composites mechanical properties is presented. Damage mode considered here includes intralaminar ply cracking that develops within the off-axis layer of a cross-ply [0/90]$_s$ and an angle-ply unbalanced symmetric [0/45]$_s$ glass fibre reinforced epoxy (GFRP) composite laminate. The strain re-distribution within the 0° plies resulting from off-axis ply cracking has been obtained experimentally using laser Raman spectroscopy (LRS). LRS provides high spatial resolution and has been proven to be a powerful tool in experimental stress and strain measurements [19–24]. Due to the poor glass fibre Raman signal, aramid fibres (Kevlar® 49) were embedded within the 0° plies and near the 0°/θ° (θ° = 90° or 45° depending on the laminate under consideration) interface as described in previous works [20–24]. Finally, the micromechanical strain mapping results are used to derive the macromechanical properties, i.e. the longitudinal modulus of elasticity. The experimental results are compared with the theoretical predictions of the ECM model [16,17] for both composite systems under consideration. The very good agreement between predicted and measured values of the reduced longitudinal Young's modulus proves that the basic assumptions of the ECM model are accurate. Since these assumptions are the basis for the calculation of the remaining mechanical properties of the laminates, it could be concluded that those model predictions are within a realistic range.

2. Experimental

Test specimens were cut from composite laminates manufactured using a modified frame-winding technique. Detailed description of the procedure can be found in the literature [23–26]. Two steel frames welded at specific angles (90° and 45°, respectively) were used for the glass fibres winding with the inner layer wound firstly on the outer frame and thus set on the second frame. The Kevlar® 49 fibres were placed at appropriate positions, 25-mm distance, on the off-axis layer and at appropriate angle to the layer orientation. Finally, after detaching the two frames the 0° layer was wound on the second frame, with the Kevlar® 49 fibre-sensors to be at the ply interface (Fig. 1). Placing the fibre-sensors at specific distance between them ensures that after cutting the tensile coupons according to ASTM D3039 standard, each coupon will contain one fibre-sensor at its mid-width. A Shell "Epicote" 828 resin was used and cured with nadic methyl-anhydride and accelerator K61B in the ratio 100:60:4. The laminate was cured between thick glass plates under 100 kg of weight for 3 h at 100 °C, followed by a post-cure at 150 °C for 3 h. The fibre volume fraction of the thus produced plates was 0.63%, the laminates ply thickness was 0.64 mm for the 0° plies and 0.61 mm for the θ° plies (θ = 45° and 90°). The laminas mechanical properties are given in Table 1. The composite material produced was transparent, which allowed the light to go through, making feasible stress and strain measurements using laser Raman spectroscopy. The thermal residual stresses introduced by the manufacturing process affect both glass fibres and Kevlar® sensors in the 0° plies. Thus, the fibre-sensors reflect in an absolute manner the real strain state within the on-axis plies and, therefore, the residual strain state arising due to cracking.

The stress state at the coupons edge has been proved to be a significant parameter for the type of cracks formed in the [0/45]$_s$ laminates [1,25]. The edge treatment affects the crack development, in a way that smoothing the edges generates unstable and rapidly growing cracks, as recent
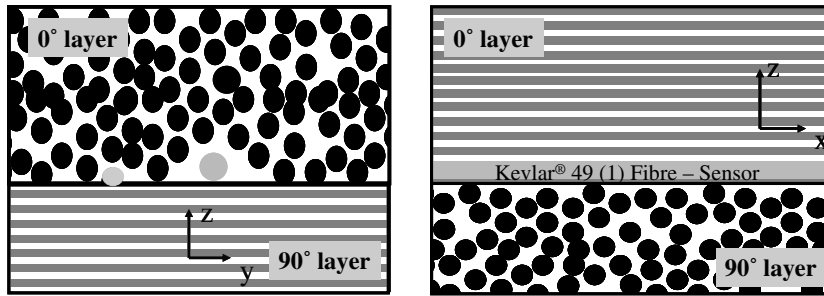
Fig. 1. A schematic figure of the composites $0°/\theta°$ area showing the position of Kevlar-49 fibre-sensors.

Table 1
Mechanical properties of the glass/epoxy composite laminas

	E_1 (GPa)	E_2(GPa)	G_{12} (GPa)	v_{12}	α_1 (°C^{-1})
0° ply	43	13	4.69	0.3	2.64×10^{-5}
90° ply	13	43	4.69	0.09	
45° ply	13.36	13.36	8.76	0.42	

research [25] showed. Notches presence at the edges facilitates crack initiation and growth from a certain position along the specimen length. Due to this effect, coupons with notches drilled, as described elsewhere [24,25], at their edges within the inner ply were used.

Strain measurements with LRS incorporates two distinct experimental methods; mechanical tensile testing for the crack pattern development and LRS for strain mapping within the 0° ply focusing mainly at the vicinity of the cracks. The mechanical tensile loading is applied through an MTS 858 Mini Bionix tester [23]. The loading rate is 0.1 mm/min to achieve controlled and stable crack growth. An electrical strain gauge has been attached on the specimen in order to monitor and control the resulting strain. Previous experimental data have shown that there is no buckling effect in the laminates under tension and thus the use of one strain gauge was considered satisfactory. The plate's initial Young's Modulus is calculated from the stress–strain curves provided by the attached strain gauge and the MTS load cell.

The technique of Raman spectroscopy, applied for the monitoring of arising strain within the 0° plies due to cracking in the $\theta°$ ply has been described elsewhere [23,24]. Here it is worth mentioning that due to the poor Raman signal of the glass-fibres, an aramid (Kevlar® 49) fibre has been placed within the 0° ply, near the $0°/\theta°$ interface, as described earlier, which thus becomes a Raman high resolution microsensor [20–24]. Using the ReRaM remote Raman system designed and developed by the Mechanics of Materials Group-FORTH/ICE-HT [19], the arising strains were derived according to the developed theory [19], which relates the shift of the Raman peaks to the applied strain or stress. The calibration curves used for deriving strain from the Raman data, employing the shift of the 1611 cm^{-1} and 1648 cm^{-1} peaks of the Kevlar® 49 Raman spectrum were presented in [26], while for the

reader's convenience are also detailed described in Appendix A.

3. Theoretical modelling

A schematic of an unbalanced symmetric $[0/\theta]_s$ composite laminate with off-axis ply matrix cracks is shown in Fig. 2. The laminate is referred to the global xyz and local $x_1x_2x_3$ co-ordinate systems, with x_1 directed along the fibres in the $\theta°$-layer. Matrix cracks are assumed to span the full width of the laminate and full thickness of the $\theta°$-layer and be spaced uniformly at a distance $2s$. It was shown in [27] that $[0/\theta]_s$ laminates can sometimes form curved cracks in the off-axis plies; however this effect is not taken into account in the model. Due to the periodicity of damage, the stress analysis may be carried out over a representative segment containing one matrix crack. Due to symmetry, it can be further restricted to one quarter of the representative segment, referred to the local co-ordinate system $x_1x_2x_3$.
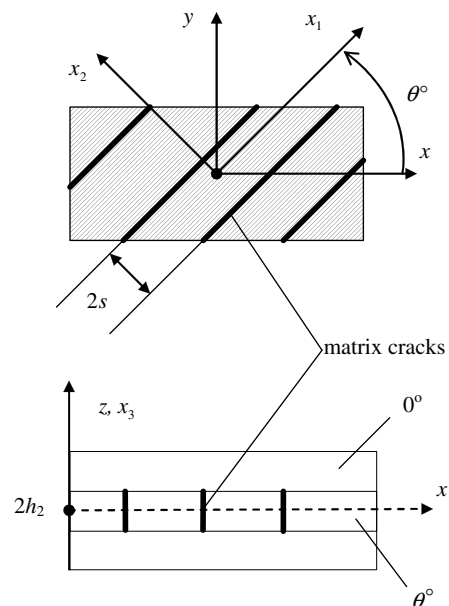

Fig. 2. Front and edge views of a $[0/\theta]_s$ laminate with off-axis ply matrix cracks.

Let $\tilde{\sigma}_{ij}^{(k)}$ and $\tilde{\varepsilon}_{ij}^{(k)}$ denote respectively the in-plane micro-stresses and microstrains in the kth layer (i.e. stresses and strains averaged across the layer thickness). The in-plane microstresses may be determined by means of a 2-D shear lag analysis [28]. The equilibrium equations in terms of microstresses take the form

$$\frac{\mathrm{d}\tilde{\sigma}_{j2}^{(2)}}{\mathrm{d}x_2} - \frac{\tau_j}{h_2} = 0, \quad j = 1, 2 \tag{1}$$

By averaging the out-of-plane constitutive equations, the interface shear stresses τ_j in Eq. (1) are expressed in terms of the in-plane displacements $\tilde{u}_{ij}^{(1)}$ and $\tilde{u}_{ij}^{(2)}$, averaged across the thickness of respectively outer and inner layers, so that

$$\tau_j = K_{j1}(\tilde{u}_1^{(2)} - \tilde{u}_1^{(1)}) + K_{j2}(\tilde{u}_2^{(2)} - \tilde{u}_2^{(1)}) \tag{2}$$

The shear lag parameters K_{11}, K_{22} and $K_{12}(\equiv K_{21})$ are determined on the assumption that the out-of-plane shear stresses vary linearly with x_3 [16–18]. Substitution of Eq. (2) into Eq. (1) and subsequent differentiation with respect to x_2 lead to the equilibrium equations in terms of in-plane microstresses and microstrains

$$\frac{\mathrm{d}^2}{\mathrm{d}x_2^2}\tilde{\sigma}_{12}^{(2)} + K_{11}(\tilde{\gamma}_{12}^{(1)} - \tilde{\gamma}_{12}^{(2)}) + K_{12}(\tilde{\varepsilon}_{22}^{(1)} - \tilde{\varepsilon}_{22}^{(2)}) = 0 \tag{3a}$$

$$\frac{\mathrm{d}^2}{\mathrm{d}x_2^2}\tilde{\sigma}_{22}^{(2)} + K_{21}(\tilde{\gamma}_{12}^{(1)} - \tilde{\gamma}_{12}^{(2)}) + K_{22}(\tilde{\varepsilon}_{22}^{(1)} - \tilde{\varepsilon}_{22}^{(2)}) = 0 \tag{3b}$$

To calculate the microstresses in the cracked lamina the constitutive equations for both layers are employed

$$
\begin{Bmatrix} \tilde{\sigma}_{11}^{(1)} \\ \tilde{\sigma}_{22}^{(1)} \\ \tilde{\sigma}_{12}^{(1)} \end{Bmatrix} = \begin{bmatrix} \widehat{Q}_{11}^{(1)} & \widehat{Q}_{12}^{(1)} & \widehat{Q}_{16}^{(1)} \\ \widehat{Q}_{12}^{(1)} & \widehat{Q}_{22}^{(1)} & \widehat{Q}_{26}^{(1)} \\ \widehat{Q}_{16}^{(1)} & \widehat{Q}_{26}^{(1)} & \widehat{Q}_{66}^{(1)} \end{bmatrix} \begin{Bmatrix} \tilde{\varepsilon}_{11}^{(1)} \\ \tilde{\varepsilon}_{22}^{(1)} \\ \tilde{\gamma}_{12}^{(1)} \end{Bmatrix} \begin{Bmatrix} \tilde{\sigma}_{11}^{(2)} \\ \tilde{\sigma}_{22}^{(2)} \\ \tilde{\sigma}_{12}^{(2)} \end{Bmatrix}
$$

$$
= \begin{bmatrix} \widehat{Q}_{11}^{(2)} & \widehat{Q}_{12}^{(2)} & 0 \\ \widehat{Q}_{12}^{(2)} & \widehat{Q}_{22}^{(2)} & 0 \\ 0 & 0 & \widehat{Q}_{66}^{(2)} \end{bmatrix} \begin{Bmatrix} \tilde{\varepsilon}_{11}^{(2)} \\ \tilde{\varepsilon}_{22}^{(2)} \\ \tilde{\gamma}_{12}^{(2)} \end{Bmatrix} \tag{4}
$$

as well as the equations of the global equilibrium of the laminate

$$
h_1 \begin{Bmatrix} \tilde{\sigma}_{11}^{(1)} \\ \tilde{\sigma}_{22}^{(1)} \\ \tilde{\sigma}_{12}^{(1)} \end{Bmatrix} + h_2 \begin{Bmatrix} \tilde{\sigma}_{11}^{(2)} \\ \tilde{\sigma}_{22}^{(2)} \\ \tilde{\sigma}_{12}^{(2)} \end{Bmatrix} = (h_1 + h_2)\bar{\sigma}_x \begin{Bmatrix} \cos^2\theta \\ \sin^2\theta \\ -\cos\theta\sin\theta \end{Bmatrix} \tag{5}
$$

assuming $\tilde{\varepsilon}_{11}^{(1)} = \tilde{\varepsilon}_{11}^{(2)}$. Finally, a system of coupled second order non-homogeneous ordinary differential equations is obtained [16,17], solutions to which are the stresses in the damaged layer:

$$\tilde{\sigma}_{j2}^{(2)} = \left(\sum_{k=1}^{2} A_{kj} \frac{\cosh\lambda_k(x_2 - s)}{\cosh\lambda_k s} + C_j\right)\bar{\sigma}_x \tag{6}$$

Here $\bar{\sigma}_x$ is the applied stress, λ_k are the roots of the characteristic equation, and A_{kj} and $C_j (j = 1, 2)$ are constants depending on the in-plane stiffness properties $[\widehat{Q}^{(1)}], [\widehat{Q}^{(2)}]$

of the intact material of the layers, shear lag parameters K_{11}, K_{22} and K_{12} and angle θ [16,18].

The in-plane microstresses in the damaged layer can be used to evaluate the reduction of the laminate stiffness properties due to damage. The constitutive equations of the homogeneous orthotropic layer equivalent to the damaged one are

$$\{\bar{\sigma}^{(2)}\} = [\bar{Q}^{(2)}]\{\bar{\varepsilon}^{(2)}\} \tag{7}$$

The lamina macrostresses $\{\bar{\sigma}^{(2)}\}$, involved in Eq. (7), are obtained by averaging the microstresses, Eq. (6), across the length of the representative segment as explicit functions of the relative crack density $D^{\mathrm{mc}} = h_2/s$

$$\bar{\sigma}_{j2}^{(2)} = \left(\sum_{k=1}^{2} A_{kj} \frac{D^{\mathrm{mc}}}{\lambda_k h_2} \tanh\frac{\lambda_k h_2}{D^{\mathrm{mc}}} + C_j\right)\bar{\sigma}_x, \quad j = 1, 2 \tag{8}$$

The macrostrains in the equivalent layer $\{\bar{\varepsilon}^{(2)}\}$ are calculated from the constitutive equations for both layers, Eq. (4), and equations of the global equilibrium of the laminate, Eq. (5), assuming $\{\bar{\varepsilon}^{(2)}\} = \{\bar{\varepsilon}^{(1)}\}$.

The in-plane stiffness matrix $[\bar{Q}^{(2)}]$ of the equivalent homogeneous layer in the local co-ordinate system is related to the in-plane stiffness matrix $[\widehat{Q}^{(2)}]$ of the undamaged material via the In-situ Damage Effective Functions (IDEFs) [28,29] $\Lambda_{jj} = \Lambda_{jj}(D^{\mathrm{mc}})$, $j = 2, 6$ as

$$[\bar{Q}^{(2)}] = [\widehat{Q}^{(2)}] - \begin{bmatrix} (\widehat{Q}_{12}^{(2)})^2/\widehat{Q}_{22}^{(2)}\Lambda_{22} & \widehat{Q}_{12}^{(2)}\Lambda_{22} & 0 \\ \widehat{Q}_{12}^{(2)}\Lambda_{22} & \widehat{Q}_{22}^{(2)}\Lambda_{22} & 0 \\ 0 & 0 & \widehat{Q}_{66}^{(2)}\Lambda_{66} \end{bmatrix} \tag{9}$$

Substituting Eq. (9) into the constitutive equations for the 'equivalent' layer, Eq. (7), gives the IDEFs Λ_{22}, Λ_{66} in terms of the lamina macrostresses $\{\bar{\sigma}^{(2)}\}$ and macrostrains $\{\bar{\varepsilon}^{(2)}\}$ as

$$\Lambda_{22} = 1 - \frac{\bar{\sigma}_{22}^{(2)}}{\widehat{Q}_{12}^{(2)}\bar{\varepsilon}_{11}^{(2)} + \widehat{Q}_{22}^{(2)}\bar{\varepsilon}_{22}^{(2)}}, \quad \Lambda_{66} = 1 - \frac{\bar{\sigma}_{12}^{(2)}}{\widehat{Q}_{66}^{(2)}\bar{\gamma}_{12}^{(2)}} \tag{10}$$

The in-plane stiffness matrix $[\bar{Q}]_2$ of the 'equivalent' layer in the global co-ordinate system xyz (Fig. 2) can be obtained from the in-plane stiffness matrix $[\bar{Q}^{(2)}]$ in the local co-ordinate system $x_1x_2x_3$ by the well-known transformation formulae [30].

4. Results and discussion

A "stop-and-go" method is employed for LRS measurements. The specimen was loaded up to a strain level where new cracks were formed, or existing cracks propagated. During the procedure the applied strain level was monitored and controlled using a strain gauge on one side of the specimen. Subsequently, it was unloaded to a strain level where the damage propagation was arrested. At such strain level, characteristic for each material (0.2% for the $[0/90]_s$ and 0.8% for the $[0/45]_s$ laminates), all the Raman measurements were collected within a so-called "window

of observation''. The cracks develop within the $\theta°$ lamina following the fibres direction. The choice of the ''window'' was based on the experiment needs, which are the observation of a crack since its formation until ''crossing'' the fibre-sensor level. Thus, in the case of [0/45]$_s$ laminates, the ''window'' should include all the cracks emanating from the drilled notches and allow the observation of their growing at least until they cross the fibre-sensor. The procedure described above has been followed in a sequence from the initiation of the first two cracks until the saturation point. In the case of [0/45]$_s$ laminates straight cracks were observed as presented in Fig. 3. The results are shown in Fig. 4 for the cross-ply and Fig. 5 for the angle-ply laminates. The strain magnification factor (SMF) measured for both composite systems reached the value of 8, which is in accordance with the expected SMF value for materials with specific degree of anisotropy [20]. Small changes observed at the SMF peaks with varying applied strain level are due to the redistribution of the strain within the 0° ply as a result of cracks interaction in addition to residual strain caused by cracking (relaxation of the thermally induced stresses during the composites manufacturing) [24].

Experimental determination of the longitudinal Young's modulus requires as the first step the recording of the 0° ply strain as affected by $\theta°$ ply cracking. This strain mapping was performed after each loading step and corresponds to the cracking patterns developed. The initial Young's Modulus has been derived according to ASTM D3039 standard, at the range of 0–0.25% of strain. The initial value of Young's Modulus of the [0/45]$_s$ laminate was 34 ± 0.57 GPa, while for the cross-ply laminate it was 29 ± 0.68 GPa. By measuring the average relative distance change between two earlier developed cracks (Figs. 4 and 5) the residual strain, after each loading step can be derived [24]. Each peak in Figs. 4 and 5 pinpoints exactly, with about 1 μm accuracy, to the centre of the corresponding crack. With the Raman technique one can determine the exact location of the crack centre with an accuracy of typically 1 μm. Hence, monitoring the relative movement of the peaks of the fibre strain distributions can perform strain measurements [24]. The procedure for residual strain measurements required strain mapping along the length of the aramid sensor at all various increments of applied strain. In each step of the procedure the displacement field
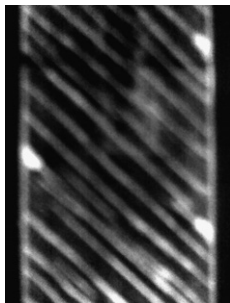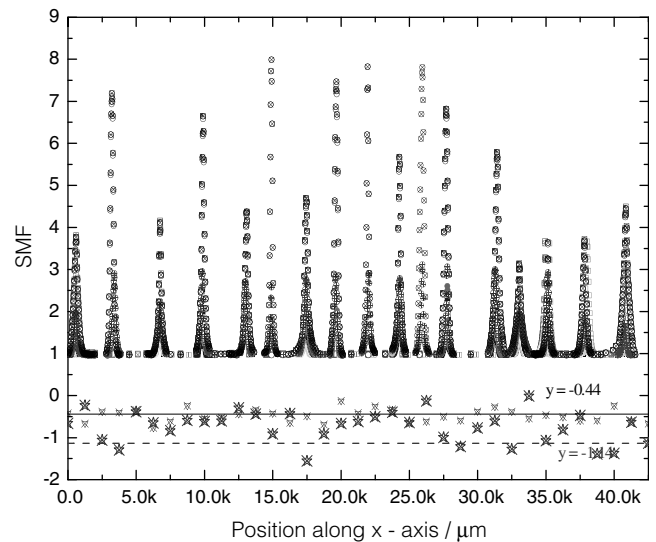

Fig. 4. Strain magnification factor within the 0° ply due to cracking in the 90° ply of a [0/90]$_s$ composite laminate with increasing level of applied strain as was monitored within the Raman ''window''.
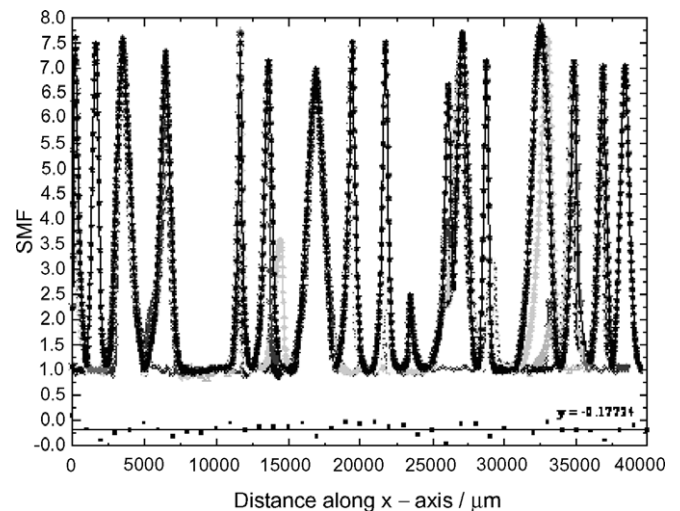

Fig. 5. Strain magnification factor within the 0° ply due to cracking in the 45° ply of a [0/45]$_s$ composite laminate with increasing level of applied strain as was monitored within the Raman ''window''.

within the Raman ''window'' due to the cracks formed was measured. The residual strain for the section of the laminate within the Raman ''window'' was measured by dividing the change in the displacement by the original Raman ''window'' gauge length. The process was repeated at every new step of applied strain. Detailed description of the procedure can be found in the literature [20–24].

The longitudinal moduli of elasticity after each level of applied strain and the corresponding developed damage state can be calculated since both the local strain and the corresponding applied stresses are known, using the displacement of the peaks in the strain profile. The laminate strain is calculated by dividing the change in displacement of the original length of the Raman ''window'' at the corresponding level of applied strain by its length (gauge length).

Fig. 3. A photograph of a portion of a [0/45]$_s$ specimen. Straight cracks are observed within the 45° ply.

This way, the modulus for the section of the laminate within the "window" was measured for each level of the increasing crack density. The reduction in stiffness is obtained by dividing the modulus derived for increasing crack densities by the initial modulus. The results for the normalised longitudinal Young's modulus are presented in Figs. 6a (cross-ply laminate) and 7a (angle-ply laminate) in tandem with the theoretical predictions of the above described ECM model. To accommodate variation in ply thickness observed in test specimens, the model was run twice – first time assuming all layers have thickness 0.61 mm, and the second 0.64 mm; however, small variation in ply thickness has very little effect on the predicted Young's modulus value. The quantity "crack density" refers to the linear crack density at each loading level, which is the number of cracks per unit length. In all cases the experimental crack density has been derived by dividing the number of the fully developed cracks to the actual "window" length. Residual strain $\{\Delta\varepsilon\}^{res}$ development in the cross-ply laminate after introducing intra-laminar cracks by mechanical loading is an elastic process caused by the different layers thermal expansion coefficients mismatch and the nature of these strains has been described elsewhere [24]. When cracks are introduced the thermally induced stresses due to manufacturing are partially relaxed. According to theory [3], the residual strain is proportional to the crack density in the non-interacting crack density region and the rate of increase is reduced when cracks become interactive [24].

The ECM model can also predict degradation of the laminate's other stiffness properties. Fig. 6b shows the predicted reduction in the shear modulus and the Poisson's ratio for a cross-ply laminate. It is obvious from comparison with Fig. 6a that degradation of these properties due to matrix cracking is more severe than that of the longitudinal Young's modulus. For crack density of 1 crack/mm, the longitudinal Young's modulus of a $[0/90]_s$ GFRP cross-ply laminate is reduced by about 20%, whereas reduction in the shear modulus is almost 40%.

In an angle-ply unbalanced $[0/45]_s$ laminate, matrix cracking, too, causes greater reduction of the transverse and shear moduli (Fig. 7b) than of the longitudinal Young's modulus (Fig. 7a), since under uniaxial tension the 0° layer still dominates the axial stiffness of the plate. For crack density of 1 crack/mm, the transverse modulus of the $[0/45]_s$ angle-ply laminate is predicted to degrade by almost 40%, whereas reduction in the shear modulus is about 25%. For this particular lay-up, small amount of matrix cracking causes reduction of the Poisson's ratio value by approximately 10% (Fig. 7c). As matrix crack density increases, however, the Poisson's ratio recovers almost to its value for the undamaged laminate. Due to its unbalanced lay-up, the $[0/45]_s$ laminate exhibits shear–extension coupling in the undamaged state, characterised by the longitudinal $\eta_{xy,x} = \bar{\gamma}_{xy}/\bar{\varepsilon}_x$ and transverse $\eta_{xy,y} = \bar{\gamma}_{xy}/\bar{\varepsilon}_y$ shear–extension coupling coefficients [30]. As matrix cracking develops in the off-axis ply, the longitudinal and transverse shear–extension coupling coefficients increase in magnitude (Fig. 7d). For higher crack densities, the transverse shear–extension coupling coefficient becomes greater than the longitudinal one, and this coincides with the recovery of the laminate's Poisson's ratio (Fig. 7c).

5. Concluding remarks

Raman spectroscopy renders a powerful tool for local strain mapping required for fundamental studies of stiffness degradation in composite laminates due to matrix cracking. The damage evolution with increasing load level can be quantified counting the strain peaks in the sensor fibre. The longitudinal modulus of cracked laminate and the residual strain are easily derived from the changes of the distance between well identified strain peaks on the sensor fibres. In the present work a comparison between experimental data and ECM model predictions is presented. The results prove that the ECM model can accurately predict reduction in the longitudinal Young's modulus due to
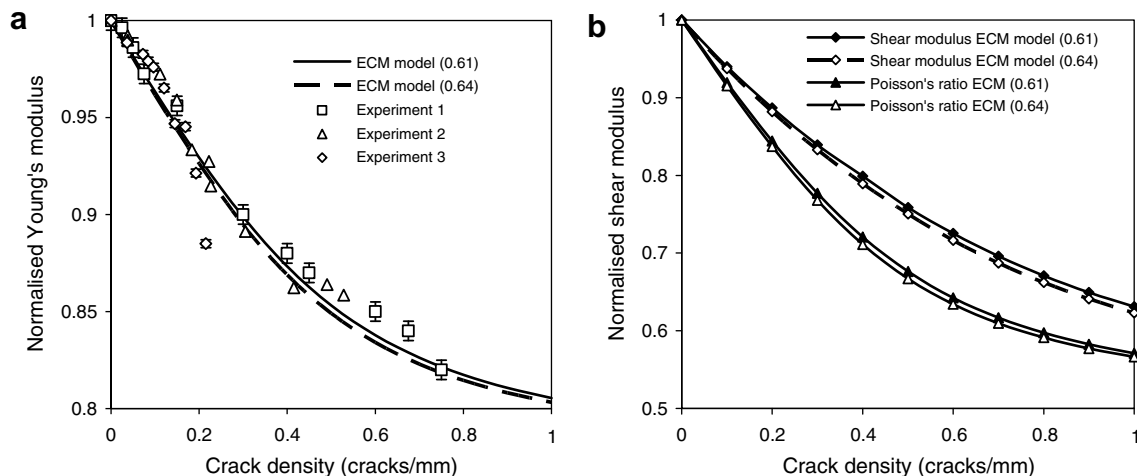

Fig. 6. Normalised stiffness properties of a $[0/90]_s$ cross-ply GFRP laminate (with a thinner or thicker ply) as a function of crack density: (a) longitudinal Young's modulus; (b) shear modulus and Poisson's ratio.
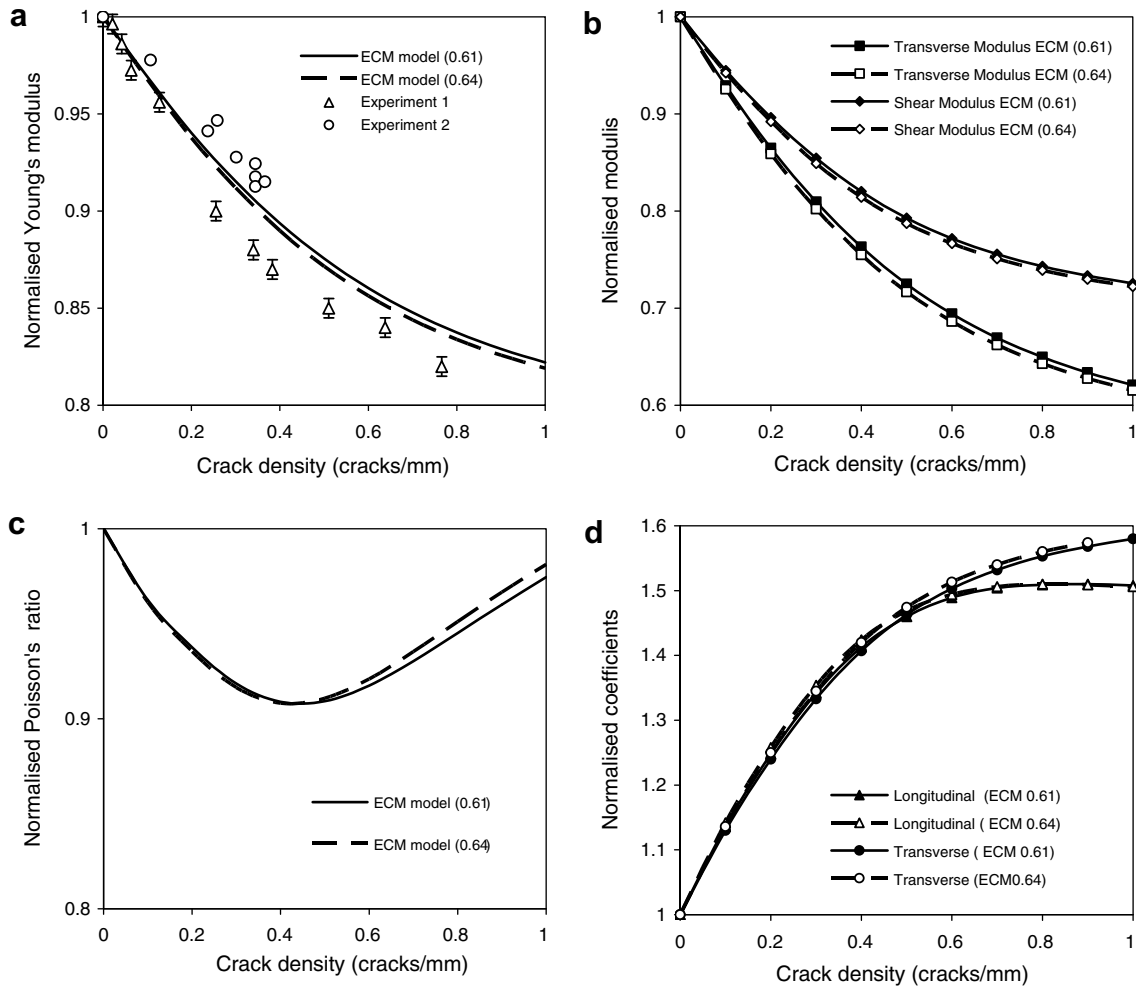
Fig. 7. Normalised stiffness properties of a [0/45]$_s$ angle-ply GFRP laminate (with a thinner or thicker ply) as a function of crack density: (a) longitudinal Young's modulus; (b) transverse and shear moduli; (c) Poisson's ratio; (d) shear–extension coupling coefficients.
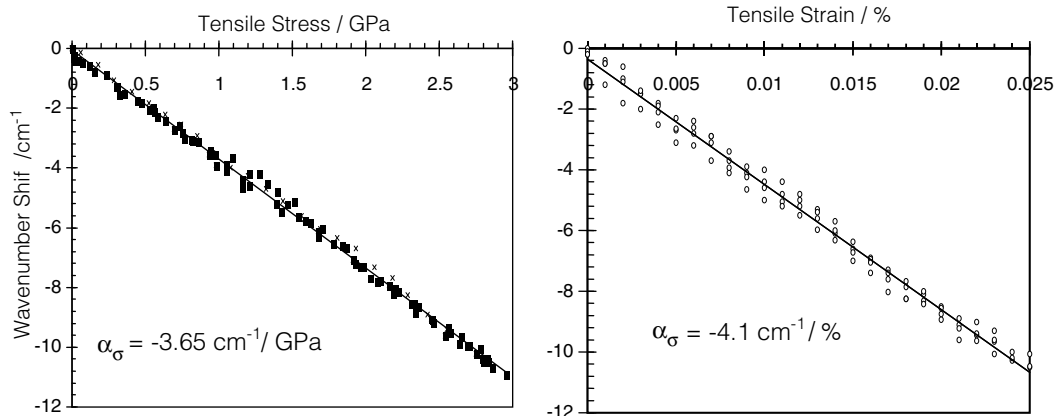

Fig. A1. Kevlar® 49 calibration curves converting Raman spectra shift to stress (a) and strain (b).

matrix cracking in both cross-ply and angle-ply laminates. The ECM model can also predict crack-induced changes of other stiffness properties such as transverse modulus, shear modulus, Poisson's ratio, shear–extension coupling coefficients. Validation of the model predictions of the Young's modulus reduction concludes that the calculations of all mechanical properties are within a realistic range. However, experimental data are required for comparison purposes, which are currently not available in the literature and this could become a task of future work.

Acknowledgements

Appendix A. Strain measurement using Raman spectroscopy

Inelastically scattered light (Raman scattering) carries important information regarding the scatterer material. Besides the data concerning chemical characteristics, LRS spectra are sensitive to the material stress and strain state. Thus, calibration curves can be drawn for each Raman active material, which correlate the shift of specific spectrum peaks to the applied stress and strain. Carbon and Kevlar® fibres that are widely used in the polymeric composites applications are excellent Raman scatterers. A general rule applied to both is that their Raman spectra shift to higher wavenumber values if the material is under compression, while they shift to lower wavenumber values when they are subjected to tension. The construction of the calibration curves for the Kevlar® 49 has been presented in the relevant literature. In the present the calibration curves as described in the [25] and showed in Fig. A1 were used for the conversion of Raman data to strain. The active Raman bands used are the peaks appearing at 1611 and 1648 wavenumbers. They are attributed mainly to stretching vibration modes of the chemical bonds between carbon atoms ($1611 \, \text{cm}^{-1}$) and carbon-oxygen atoms ($1648 \, \text{cm}^{-1}$).

References

[1] Talreja R. Damage characterization by internal variables. In: Pipes RB, Talreja R, editors. Composite materials series. Damage mechanics of composite materials, vol. 9. Amsterdam: Elsevier; 1994.

[2] Nairn J, Hu S. Matrix microcracking. In: Pipes RB, Talreja R, editors. Composite materials series. Damage mechanics of composite materials, vol. 9. Amsterdam: Elsevier; 1994.

[3] Nairn J. Matrix microcracking in composites. In: Kelly A, Zweben C, Talreja R, Manson J-A, editors. Comprehensive composite materials. Polymer matrix composites, vol. 2. Amsterdam: Elsevier; 2000.

[4] Varna J, Joffe R, Akshantala NV, Talreja R. Damage in composite laminates with off-axis plies. Comp Sci Tech 1999;59(14):2139–47.

[5] Kashtalyan M, Soutis C. Analysis of composite laminates with intra- and interlaminar damage. Progr Aerosp Sci 2005;41(2):152–73.

[6] Hashin Z. Analysis of cracked laminates: a variational approach. Mech Mater 1985;4(2):121–36. 1985.

[7] Schoeppner GA, Pagano N. Stress fields and energy release rates in cross-ply laminates. Int J Sol Struct 1998;35(11):1025–55.

[8] McCartney LN, Schoeppner GA, Becker W. Comparison of models for transverse ply cracks in composite laminates. Comp Sci Tech 2000;60(12–13):2347–59.

[9] Tong J, Guild FJ, Ogin SL, Smith PA. On matrix crack growth in quasi-isotropic laminates – II Finite element analysis. Comp Sci Tech 1997;57(11):1537–45.

[10] Marsden WM, Guild FJ, Ogin SL, Smith PA. Modelling stiffness-damage behaviour of ($\pm45/90$)$_s$ and ($90/\pm45$)$_s$ glass fibre reinforced polymer laminates. Plast Rub Comp 1999;28(1):30–9.

[11] Pradhan B, Venu Kumar N, Rao NS. Stiffness degradation resulting from 90° ply cracking in angle-ply composite laminates. Comp Sci Tech 1999;59(10):1543–52.

[12] Gudmundson P, Östlund S. First order analysis of stiffness reduction due to matrix cracking. J Comp Mater 1992;26(7):1009–30.

[13] Gudmundson P, Zang W. A universal model for thermoelastic properties of macro cracked composite laminates. Int J Sol Struct 1993;30(23):3211–31.

[14] Lundmark P, Varna J. Constitutive relationships for damaged laminate in in-plane loading. Int J Dam Mech 2005;14(3):235–59.

[15] Lundmark P, Varna J. Crack face sliding effect on stiffness of laminates with ply cracks. Comp Sci Tech 2006;66(10):1444–54.

[16] Kashtalyan M, Soutis C. Stiffness degradation in cross-ply laminates damaged by transverse cracking and splitting. Comp Part A: Appl Sci Manuf 2000;31(4):335–51.

[17] Kashtalyan M, Soutis C. Modelling stiffness degradation due to matrix cracking in angle-ply composite laminates. Plastics, Rubber Compos 2000;29(9):482–8.

[18] Kashtalyan M, Soutis C. Modelling off-axis matrix cracking in continuous fibre-reinforced polymer matrix composite laminates. J Mater Sci 2006;41(20):6789–99.

[19] Paipetis A, Vlattas C, Galiotis C. Remote laser Raman microscopy (ReRaM); Part 1 Design and testing of a confocal microprobe. J Raman Spectrosc 1996;27(7):519–26.

[20] Katerelos DTG, Galiotis C. Experimental determination of stress concentrations in composite laminates and their effects on damage evolution. Applied mechanics and materials, vols. 5–6. Switzerland: Trans Tech Publications; 2006. p. 383–90.

[21] Katerelos DG, Parthenios J, Galiotis C. Strain redistribution in composite laminates resulting from off-axis ply cracking. In: Gdoutos EE, Margioli-Riga Z, editors. Recent advances in composite materials – In honor of S.A. Paipetis. Dordrecht: Kluwer; 2003.

[22] Katerelos DG, Galiotis C. Axial strain redistribution resulting from off-axis ply cracking in polymer composites. App Phys Lett 2004;85(17):3752–4.

[23] Katerelos DG, McCartney LN, Galiotis C. Local strain re-distribution and stiffness degradation in cross-ply polymer composites under tension. Acta Mater 2005;53(12):3335–43.

[24] Katerelos DTG, Lundmark P, Varna J, Galiotis C. Analysis of matrix cracking in GFRP laminates using Raman spectroscopy. Comp Sci Tech 2006;67(9):1946–54.

[25] Crocker LE, Ogin SL, Smith PA, Hill PS. Intra-laminar fracture in angle-ply laminates. Comp Part A 1997;28A(9–10):839–46.

[26] Parthenios J, Katerelos DG, Psarras GC, Galiotis C. Aramid fibres; a multifunctional sensor for monitoring stress/strain fields and damage development in composite materials. Eng Fract Mech 2002;69(9):1067–78.

[27] O'Brien TK, Hooper SJ. Local delamination in laminates with angle ply matrix cracks: Part I Tension test and stress analysis. NASA Technical memorandum 104055/AVSCOM Technical Report 91-B-010; 1991.

[28] Zhang J, Fan J, Soutis C. Analysis of multiple matrix cracking in composite laminates. Part 1: In-plane stiffness properties. Composites 1992;23(9):291–8.

[29] Fan J, Zhang J. In-situ damage evolution and micro/macro transition for laminated composites. Compos Sci Technol 1993;47(3):107–18.

[30] Jones RM. Mechanics of composite materials. 2nd ed. Philadelphia PA: Francis & Taylor; 1999.